Electronic Supplementary Material associated with

A Heterobimetallic Au(I)–Ru(II) Complex Bridged by dppb: Synthesis, Structural and Solution Characterization, BSA Interaction and *In Vivo* Toxicity Evaluation in Wistar Rats

Adnan Zahirović[1]*, Sunčica Roca[2], Muhamed Fočak[3], Selma Fetahović[1], Višnja Muzika[4], Damir Suljević[2], Anela Topčagić[1], Maja Mitrašinović Brulić[2], Irnesa Osmanković[1], Debbie C. Crans[5] and Aleksandar Višnjevac[2]*

[1] Laboratory for Inorganic and Bioinorganic Chemistry, Department of Chemistry, Faculty of Science, University of Sarajevo, Bosnia and Herzegovina
[2] Ruđer Bošković Institute, Zagreb, Croatia
[3] Department of Biology, Faculty of Science, University of Sarajevo, Bosnia and Herzegovina
[4] Department of Histology and Embryology, Faculty of Medicine, University of Sarajevo, Bosnia and Herzegovina
[5] Department of Chemistry and Cell & Molecular Biology Program, Colorado State University, Fort Collins, USA

***Correspondence should be sent to:**
adnan.zahirovic@pmf.unsa.ba
aleksandar.visnjevac@irb.hr

Contents

Figure S1. Infrared spectra of dppb, $[RuCl_2(p\text{-cymene})]_2$, $[\{RuCl_2(p\text{-cymene})\}_2(\mu\text{-dppb})]$, $[Au_2Cl_2(dppb)_2]$ and AuRu. 3

Table S1. Characteristic IR vibrations. 3

Figure S2. Electron spectra of complexes $[\{RuCl_2(p\text{-cymene})\}_2(\mu\text{-dppb})]$, $[Au_2Cl_2(dppb)_2]$, AuRu. and dppb ligand at concentrations 1×10^{-5} M recorded in dichloromethane. 5

Table S2. Electron transitions in spectra of complexes $[RuCl_2(p\text{-cymene})(dppb)]_2$, $[Au_2Cl_2(dppb)_2]$, AuRu. and dppb ligand. 5

Figure S3. 600.130 MHz ^{1}H NMR spectrum of the AuRu with signals labeled according to the numbering in the schematic representation of the complex structure (solvent: CD_2Cl_2-d_2, temperature: 25 °C, the signals were calibrated against the solvent signal $\delta_{1H} = 5.32$ ppm). 7

Figure S4. 600 MHz H,H-COSY NMR spectrum of AuRu**.** At the left edge and top is the one-dimensional ^{1}H NMR spectrum with assignments. On the left side, a part of the spectrum is shown separately and zoomed for clarity (solvent: CD_2Cl_2-d_2, temperature: 25 °C, the signals were calibrated against the solvent signal $\delta_{1H} = 5.32$ ppm). 8

Figure S5. 600 MHz H,H-NOESY NMR spectrum of AuRu**.** At the left edge and top is the one-dimensional ^{1}H NMR spectrum with assignments (solvent: CD_2Cl_2-d_2, temperature: 25 °C, the signals were calibrated against the solvent signal $\delta_{1H} = 5.32$ ppm). 9

Figure S6. 2D H,C-HMQC NMR spectrum of AuRu. The 1D 600 MHz ^{1}H NMR spectrum is shown at the top and the 150 MHz ^{13}C spectrum at the left. For clarity, two parts of the spectrum are shown separately and zoomed (solvent: CD_2Cl_2-d_2, temperature: 25 °C, the signals were calibrated against the solvent signal $\delta_{1H} = 5.32$ ppm and $\delta_{13C} = 54.00$ ppm). 10

Figure S7. 2D H,C-HMBC NMR spectrum of AuRu. The 1D 600 MHz ^{1}H NMR spectrum is shown at the top and the 150 MHz ^{13}C spectrum at the left. For clarity, part of the spectrum is shown separately and zoomed (solvent: CD_2Cl_2-d_2, temperature: 25 °C, the signals were calibrated against the solvent signal δ_{1H} = 5.32 ppm and δ_{13C} = 54.00 ppm). 11

Figure S8. 150.903 MHz $^{13}C\{^{1}H\}$ NMR spectrum of AuRu with signals marked according to the numbering in the schematic representation of the complex structure (solvent: CD_2Cl_2-d_2, temperature: 25 °C, the signals were calibrated against the solvent signal δ_{13C} = 54.00 ppm). 12

Figure S9. 242.925 MHz ^{31}P NMR spectrum of AuRu with signals labeled according to the metal ion to which the phosphorus atom is bound (solvent: CD_2Cl_2-d_2, temperature: 25 °C, the δ-scale is related to the external standard signal of 85% H_3PO_4, δ_{31P} = 0.0 ppm). 13

Figure S10. .Interaction of $[Au_2Cl_2(dppb)_2]$ with BSA in 50 mM phosphate buffer pH 7.42: a) fluorescence quenching of BSA (2.93×10^{-5} M) in the presence of increasing concentration of $[Au_2Cl_2(dppb)_2]$; b) graphical determination of Stern–Volmer constant; c) graphical determination of binding constant and the number of binding sites. 14

Figure S11. Interaction of $[\{RuCl_2(p\text{-cymene})\}_2(\mu\text{-dppb})]$ with BSA in 50 mM phosphate buffer pH 7.42: a) fluorescence quenching of BSA (2.93×10^{-5} M) in the presence of increasing concentration of complex; b) graphical determination of Stern–Volmer constant; c) graphical determination of binding constant and the number of binding sites. 14

Figure S12. Overlap of the BSA emission spectrum and absorption spectrum of $[Au_2Cl_2(dppb)_2]$..... 15

Figure S13. Overlap of the BSA emission spectrum and absorption spectrum of $[\{RuCl_2(p\text{-cymene})\}_2(\mu\text{-dppb})]$. 15

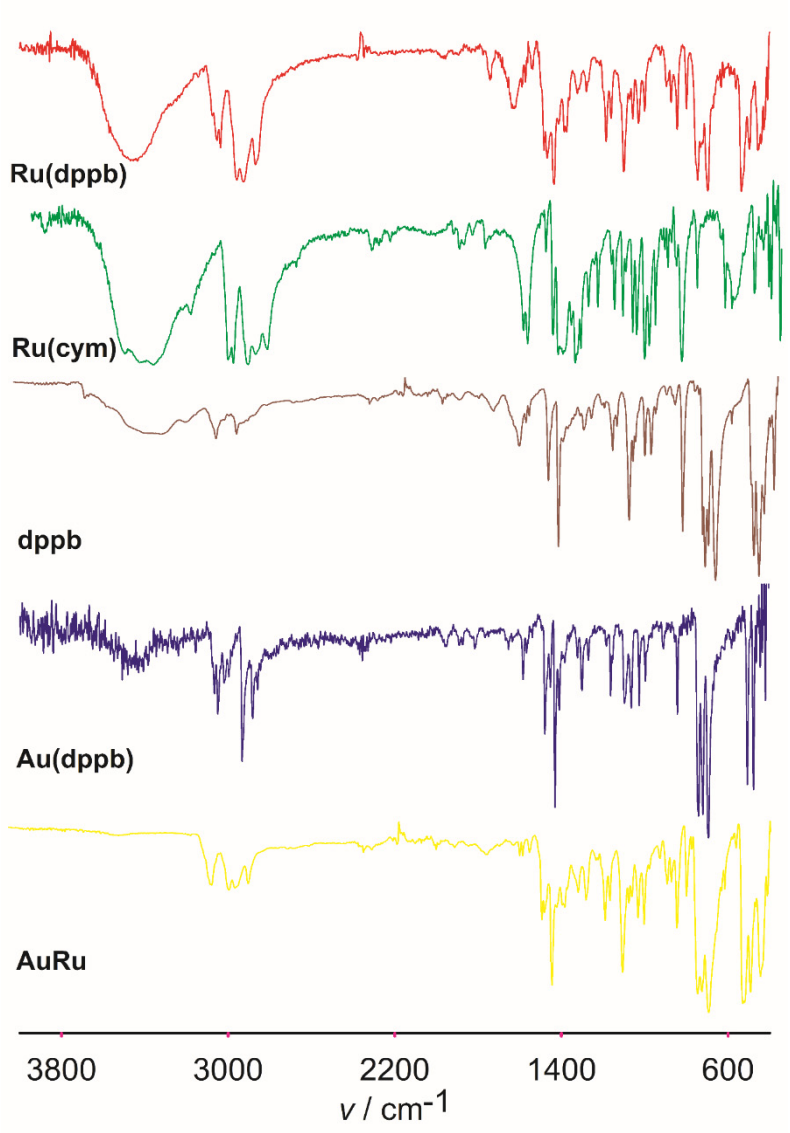


Figure S1. Infrared spectra of dppb, $[RuCl_2(p\text{-cymene})]_2$, $[\{RuCl_2(p\text{-cymene})\}_2(\mu\text{-dppb})]$, $[Au_2Cl_2(dppb)_2]$ and AuRu.

Table S1. Characteristic IR vibrations.

Compound	$\nu(C–H)_{aryl}$	$\nu(C–H)_{alkyl}$	CH_2 scissoring	$\nu(P–C)_{aryl}$	CH_2 rocking	$\gamma(C–H)_{out\text{-}of\text{-}plane}$ of *p*-cimene aromatic ring	$\gamma(C–H)_{out\text{-}of\text{-}plane}$ of dppb aromatic rings and $\nu(P–C)_{alkyl}$, fingerprint region
	cm^{-1}						
Ru(dppb)	3053, 3034	2957, 2924, 2866	1434	1099	842	797	744, 719, 695
Ru(cym)	3055, 3030	2961, 2924, 2868	n.a.	n.a.	n.a.	803	n.a.
dppb	3063, 3047, 3018	2932, 2881, 2858	1430	1096	842	n.a.	742, 721, 695
Au(dppb)	3061, 3047	2950, 2914, 2895	1434	1100	848	n.a.	742, 727, 693
AuRu	3047, 3038	2959, 2931, 2913, 2868	1432	1100	848	797	745, 726, 693

Figure S1 presents the infrared spectra of the AuRu complex alongside those of dppb, $[RuCl_2(p\text{-cymene})]_2$, $[\{RuCl_2(p\text{-cymene})\}_2(\mu\text{-dppb})]$ and $[Au_2Cl_2(dppb)_2]$ (complexes are abbreviated as Ru(cym), Ru(dppb) and Au(dppb), respectively). The corresponding vibrational assignments relevant to ligand coordination are summarized in the Table S1. The absorption bands observed in the region between 3000 and 3070 cm^{-1} across all spectra are attributed to the stretching vibrations of aromatic C–H bonds, which originate either from the *p*-cymene moiety or from the phenyl rings of the dppb ligand. In contrast, the bands located in the range of 2960 to 3000 cm^{-1} are associated with C–H stretching vibrations of aliphatic groups, specifically arising from the alkyl chain of dppb and the methyl and isopropyl substituents present in the *p*-cymene structure. The IR spectrum of free dppb exhibits distinctive bands at 742, 721, and 695 cm^{-1}, which are ascribed to out-of-plane bending vibrations of C–H bonds in monosubstituted phenyl rings, as well as to stretching vibrations involving the $P–C_{alkyl}$ bonds. These characteristic vibrational modes are also discernible in the spectra of the AuRu complex, Ru(dppb), and Au(dppb), thereby providing strong evidence for the successful coordination of the dppb ligand to the metal centers, as detailed in the Table S1. Additionally, the $P–C_{aryl}$ stretching vibration, which appears at 1096 cm^{-1} in the spectrum of uncoordinated dppb, is slightly shifted to 1098 cm^{-1} in both AuRu and Ru(dppb), and to 1100 cm^{-1} in Au(dppb). This shift, accompanied by an increase in band intensity, reflects a reduction in electron density on the phosphorus atoms upon coordination to the metal centers. Furthermore, the CH_2 scissoring mode, initially observed at 1430 cm^{-1} in the free ligand, is shifted to 1432 cm^{-1}, 1434 cm^{-1}, and 1432 cm^{-1} in the respective spectra of the three complexes. Similarly, the rocking vibration of the CH_2 groups, originally positioned at 842 cm^{-1} in dppb, is detected at 842 cm^{-1}, 848 cm^{-1}, and 842 cm^{-1} in the corresponding complexes. The spectra of Ru(cym), AuRu, and Ru(dppb) exhibit an additional band at 803, 797, and 797 cm^{-1}, respectively, which is attributed to an out-of-plane bending vibration of the C–H bond within the aromatic ring of *p*-cymene. The presence of this vibrational mode confirms the coordination of the *p*-cymene ligand to the ruthenium center in the synthesized AuRu complex.

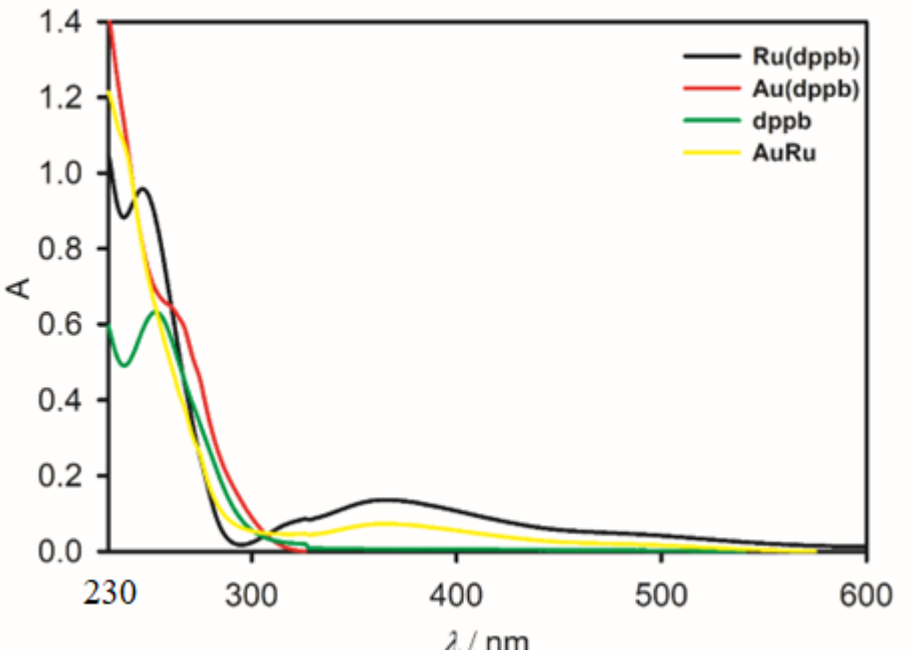


Figure S2. Electron spectra of complexes [{$RuCl_2$(*p*-cymene)}$_2$(μ-dppb)], [Au_2Cl_2(dppb)$_2$], AuRu. and dppb ligand at concentrations 1×10^{-5} M recorded in dichloromethane.

Table S2. Electron transitions in spectra of complexes [$RuCl_2$(*p*-cymene)(dppb)]$_2$, [Au_2Cl_2(dppb)$_2$], AuRu. and dppb ligand.

Compound	π→π*	n→π*	LMCT	d–d
		λ/nm (logε)		
dppb	<230	258 (4.08)	n.a.	n.a.
Ru(dppb)	<230	255 (4.21)	361 (3.43)	500 (2.51)
Au(dppb)	<230	269 (4.04)	n.a.	n.a.
AuRu	240 (4.31)	268 (3.86)	362 (3.16)	500 (2.92)

The electronic spectra of the free dppb ligand, as well as those of the complexes Au(dppb), Ru(dppb), and the heterobimetallic AuRu species, are presented in Figure S2, with the corresponding absorption maxima listed in Table S2. In the spectrum of the AuRu complex, an intense absorption band at 240 nm can be attributed to π→π* transitions within the aromatic rings of both the dppb ligand and the p-cymene moiety, while analogous transitions in the spectra of the individual complexes and the free ligand appear at slightly shorter wavelengths (<230 nm). All spectra also exhibit an absorption feature in the 255–270 nm region, assigned to an n→π* transition involving donation of the phosphorus lone pair into the π* orbitals of the aromatic system, thereby providing spectroscopic evidence for successful coordination. More importantly, the AuRu spectrum reveals a distinct absorption band at 362 nm, essentially coincident with the feature observed at 361 nm in the Ru(dppb) complex. This transition can be ascribed to a ligand-to-metal charge transfer (LMCT) process involving the chloride ligands and the Ru(II) center, in full agreement with previously reported spectra of chloro-ruthenium(II) arene complexes. In addition, a weak band centered around 500 nm is observed in both the Ru(dppb) and AuRu complexes, characteristic of d–d transitions at the low-spin d^6 Ru(II) center. The invariance of this band in the two spectra indicates that the coordination environment around ruthenium, and hence the associated crystal-field splitting parameters, remain essentially unchanged upon introduction of the gold fragment.

Conductivity measurements show that the molar conductivity of the AuRu complex in DMSO solution at 25 °C is 9.2 S cm^2 mol^{-1}, consistent with its non-electrolytic nature.

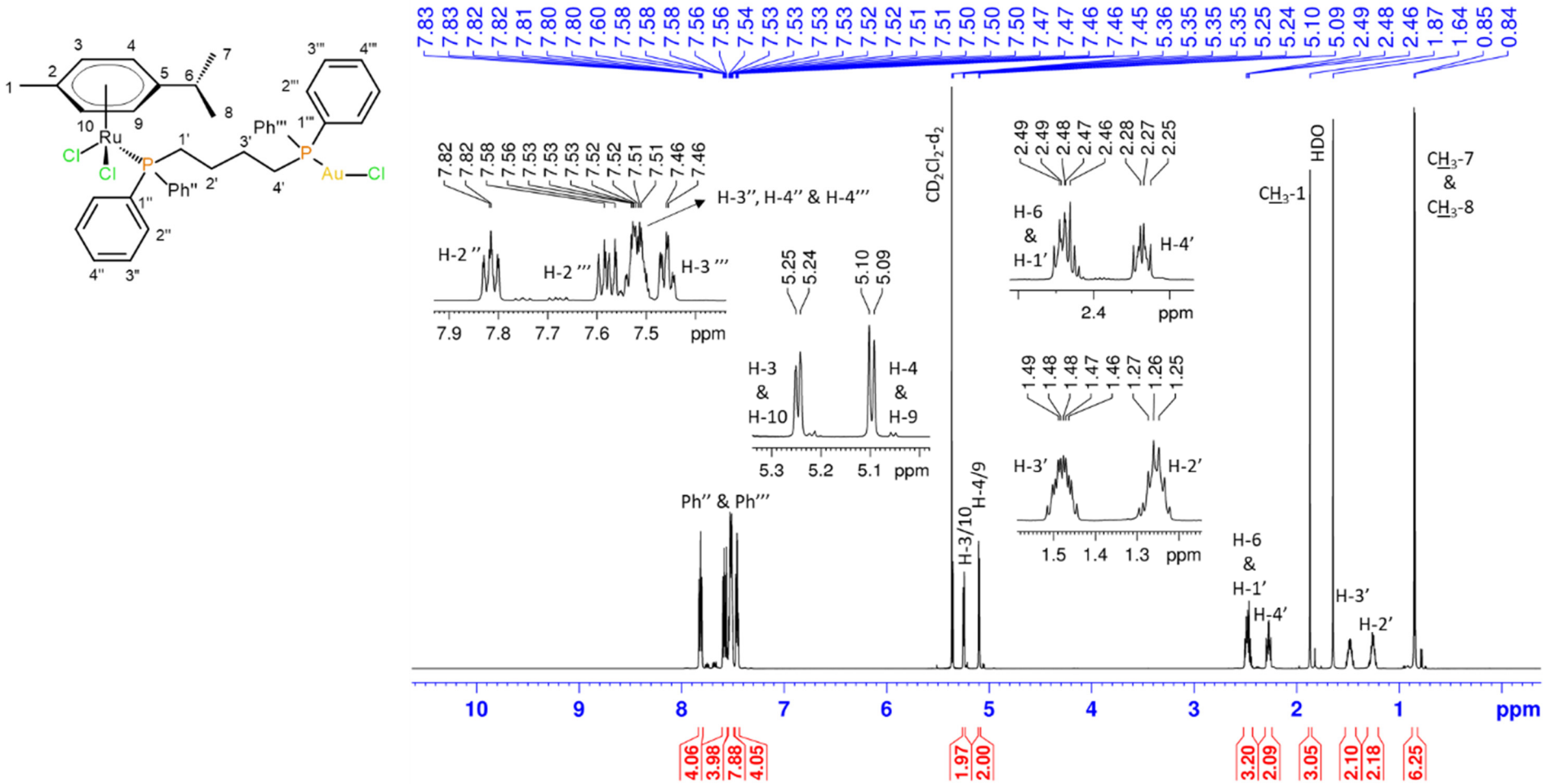


Figure S3. 600.130 MHz ^{1}H NMR spectrum of the AuRu with signals labeled according to the numbering in the schematic representation of the complex structure (solvent: CD_2Cl_2-d_2, temperature: 25 °C, the signals were calibrated against the solvent signal δ_{1H} = 5.32 ppm).

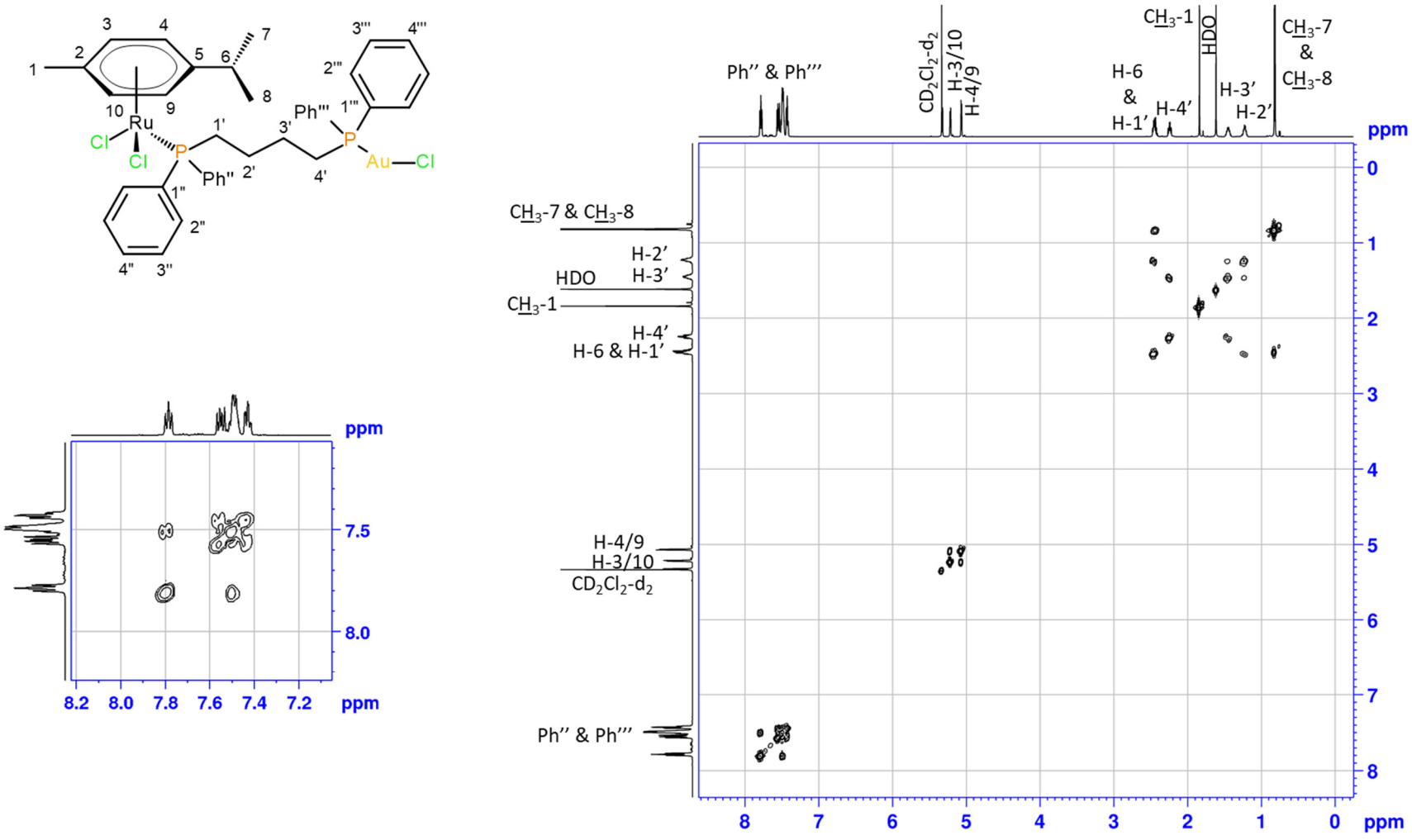


Figure S4. 600 MHz H,H-COSY NMR spectrum of AuRu**.** At the left edge and top is the one-dimensional ^{1}H NMR spectrum with assignments. On the left side, a part of the spectrum is shown separately and zoomed for clarity (solvent: CD_2Cl_2-d_2, temperature: 25 °C, the signals were calibrated against the solvent signal δ_{1H} = 5.32 ppm).

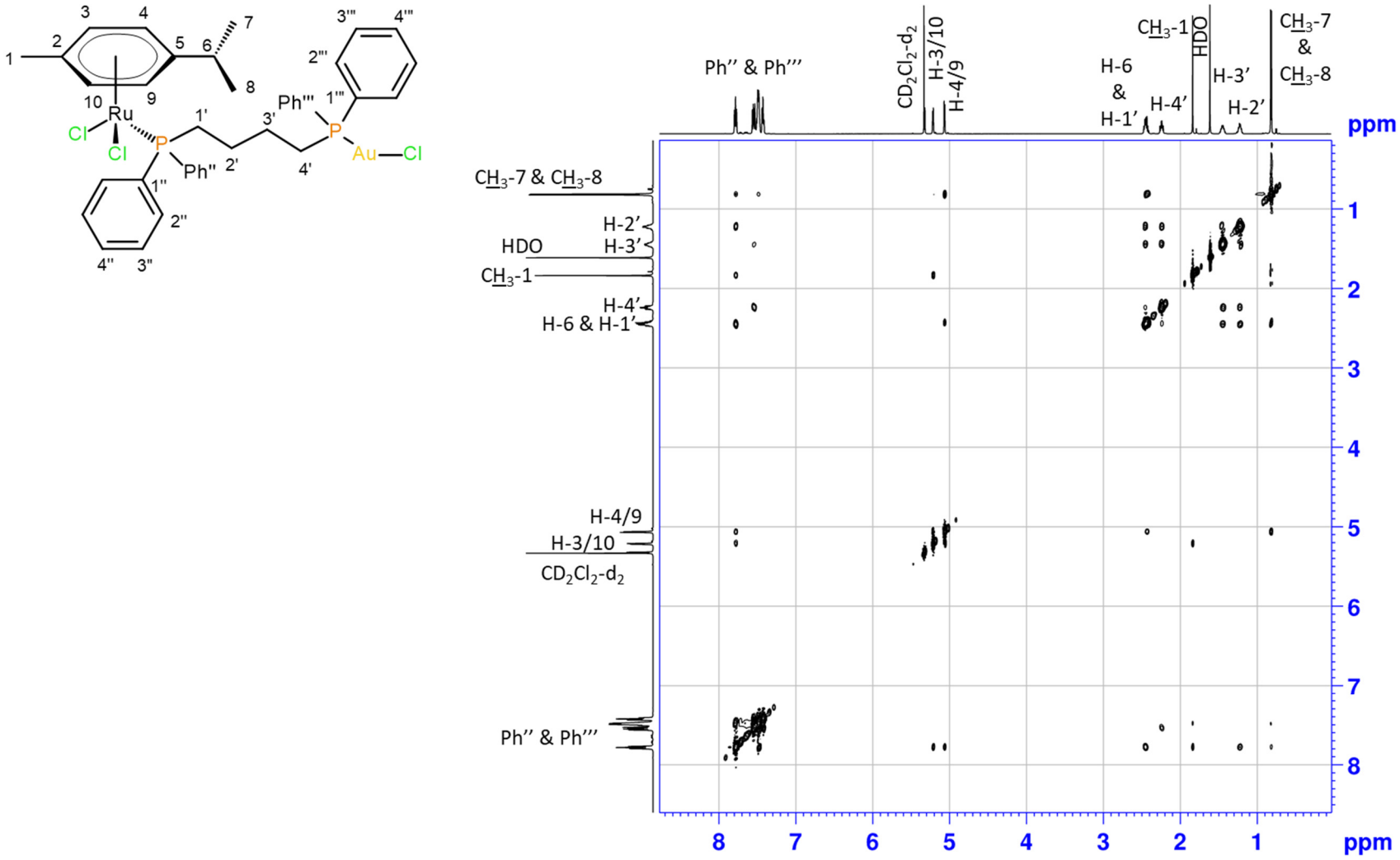


Figure S5. 600 MHz H,H-NOESY NMR spectrum of AuRu**.** At the left edge and top is the one-dimensional ^{1}H NMR spectrum with assignments (solvent: CD_2Cl_2-d_2, temperature: 25 °C, the signals were calibrated against the solvent signal δ_{1H} = 5.32 ppm).

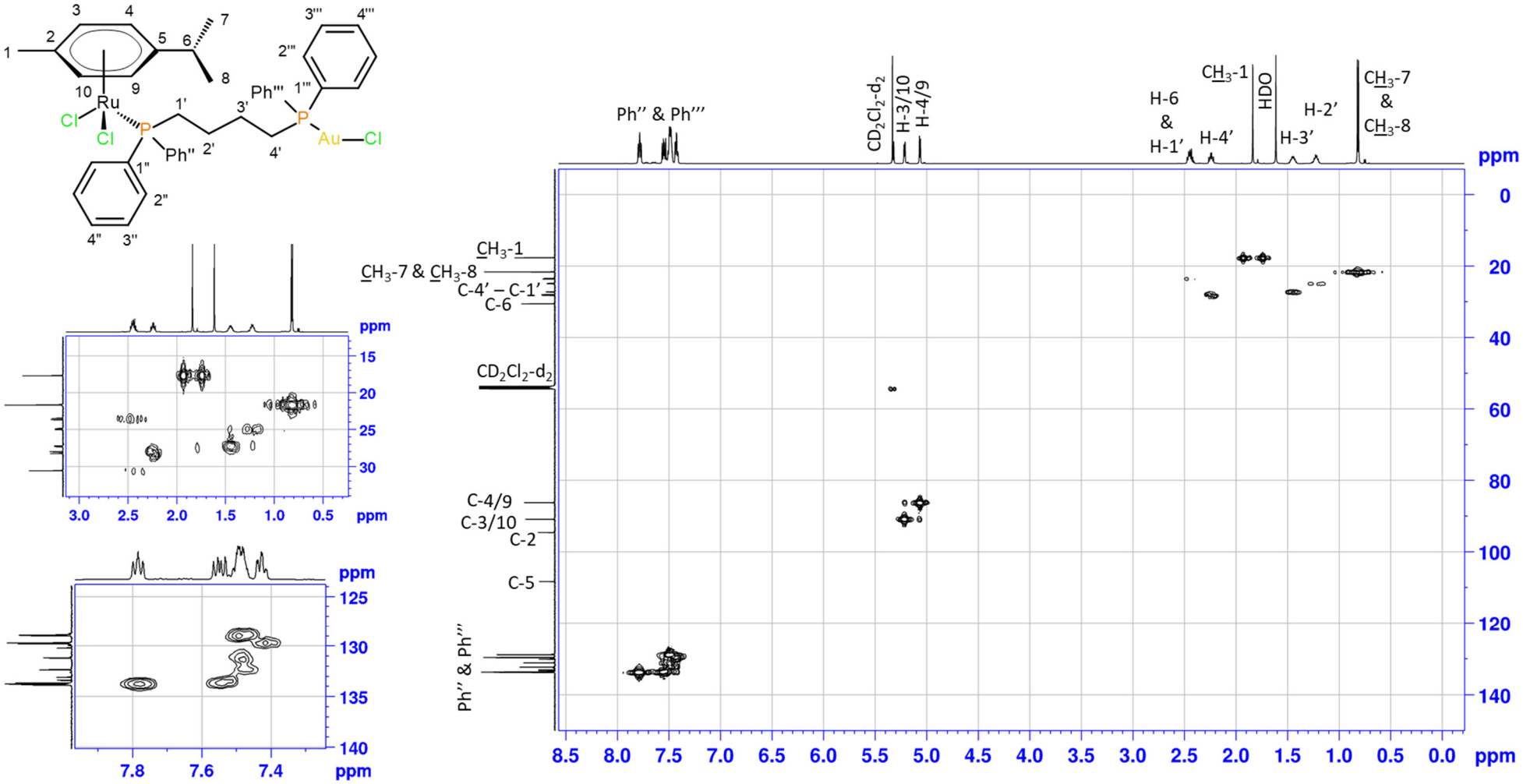


Figure S6. 2D H,C-HMQC NMR spectrum of AuRu. The 1D 600 MHz ^{1}H NMR spectrum is shown at the top and the 150 MHz ^{13}C spectrum at the left. For clarity, two parts of the spectrum are shown separately and zoomed (solvent: CD_2Cl_2-d_2, temperature: 25 °C, the signals were calibrated against the solvent signal δ_{1H} = 5.32 ppm and δ_{13C} = 54.00 ppm).

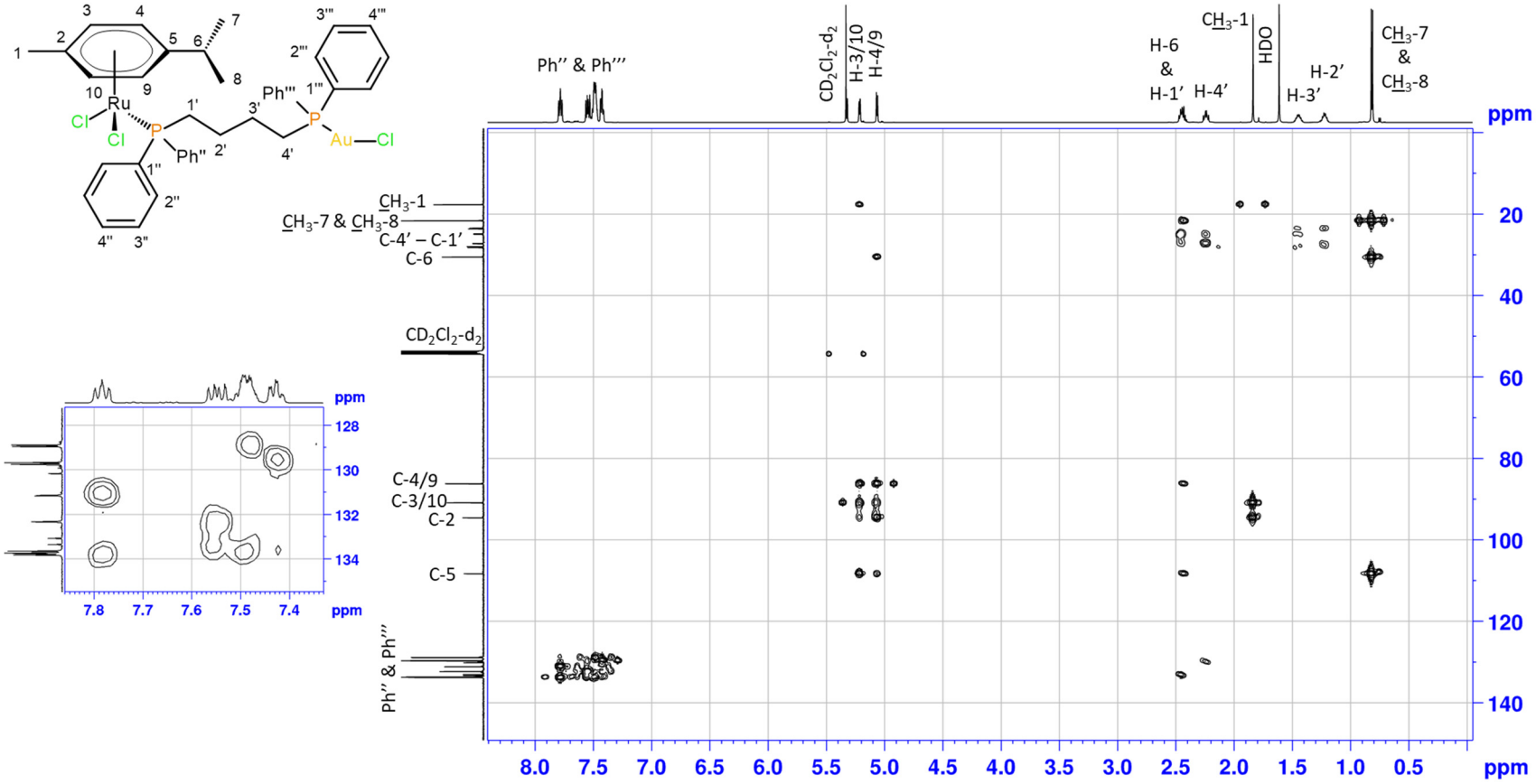


Figure S7. 2D H,C-HMBC NMR spectrum of AuRu. The 1D 600 MHz ^{1}H NMR spectrum is shown at the top and the 150 MHz ^{13}C spectrum at the left. For clarity, part of the spectrum is shown separately and zoomed (solvent: CD_2Cl_2-d_2, temperature: 25 °C, the signals were calibrated against the solvent signal δ_{1H} = 5.32 ppm and δ_{13C} = 54.00 ppm).

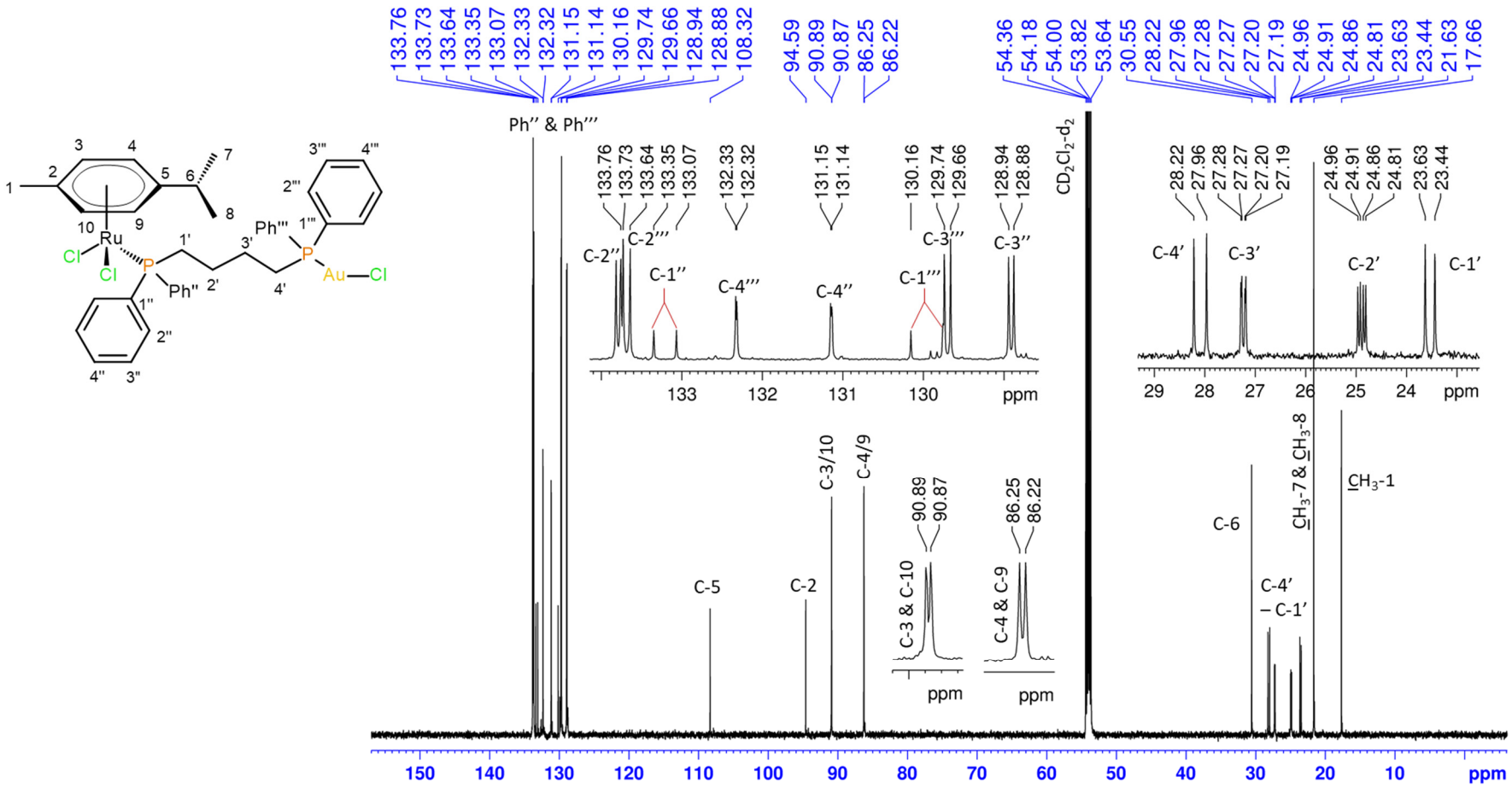


Figure S8. 150.903 MHz $^{13}C\{^{1}H\}$ NMR spectrum of AuRu with signals marked according to the numbering in the schematic representation of the complex structure (solvent: CD_2Cl_2-d_2, temperature: 25 °C, the signals were calibrated against the solvent signal δ_{13C} = 54.00 ppm).

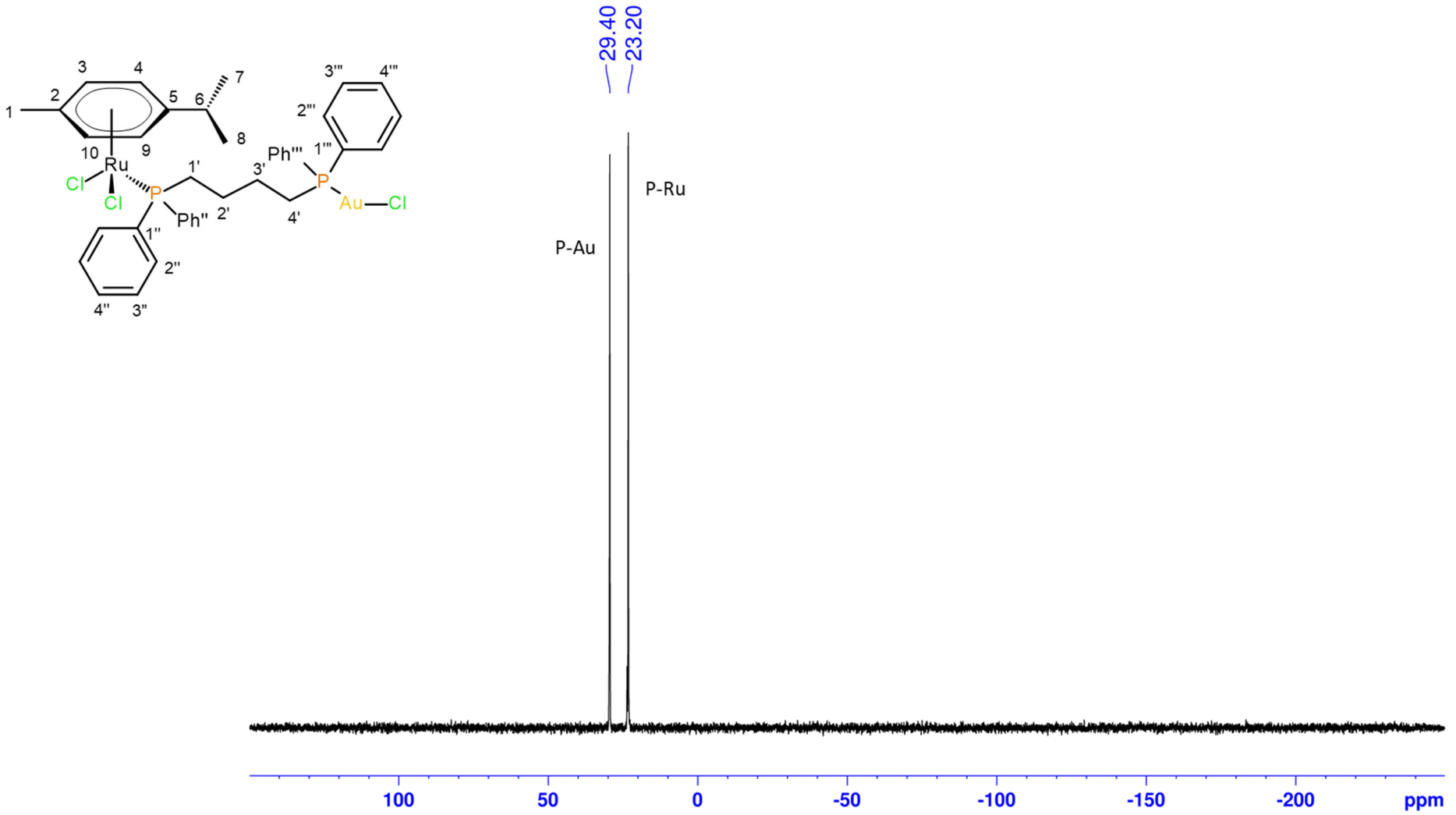


Figure S9. 242.925 MHz ^{31}P NMR spectrum of AuRu with signals labeled according to the metal ion to which the phosphorus atom is bound (solvent: CD_2Cl_2-d_2, temperature: 25 °C, the δ-scale is related to the external standard signal of 85% H_3PO_4, δ_{31P} = 0.0 ppm).

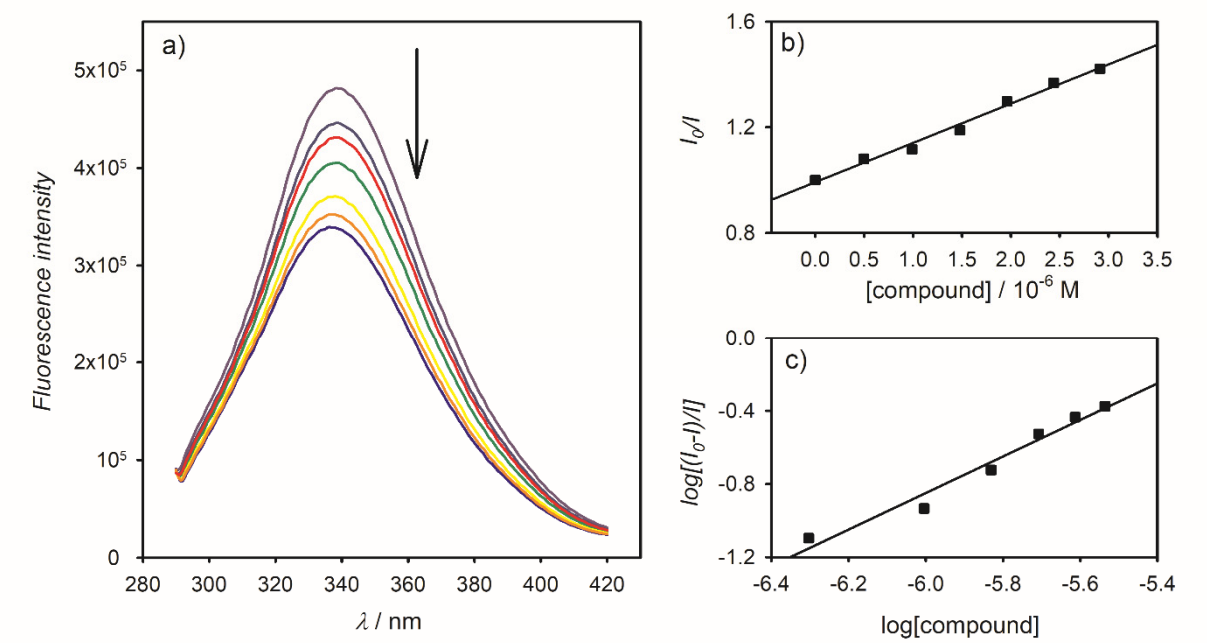


Figure S10. .Interaction of $[Au_2Cl_2(dppb)_2]$ with BSA in 50 mM phosphate buffer pH 7.42: a) fluorescence quenching of BSA (2.93×10^{-5} M) in the presence of increasing concentration of $[Au_2Cl_2(dppb)_2]$; b) graphical determination of Stern–Volmer constant; c) graphical determination of binding constant and the number of binding sites.

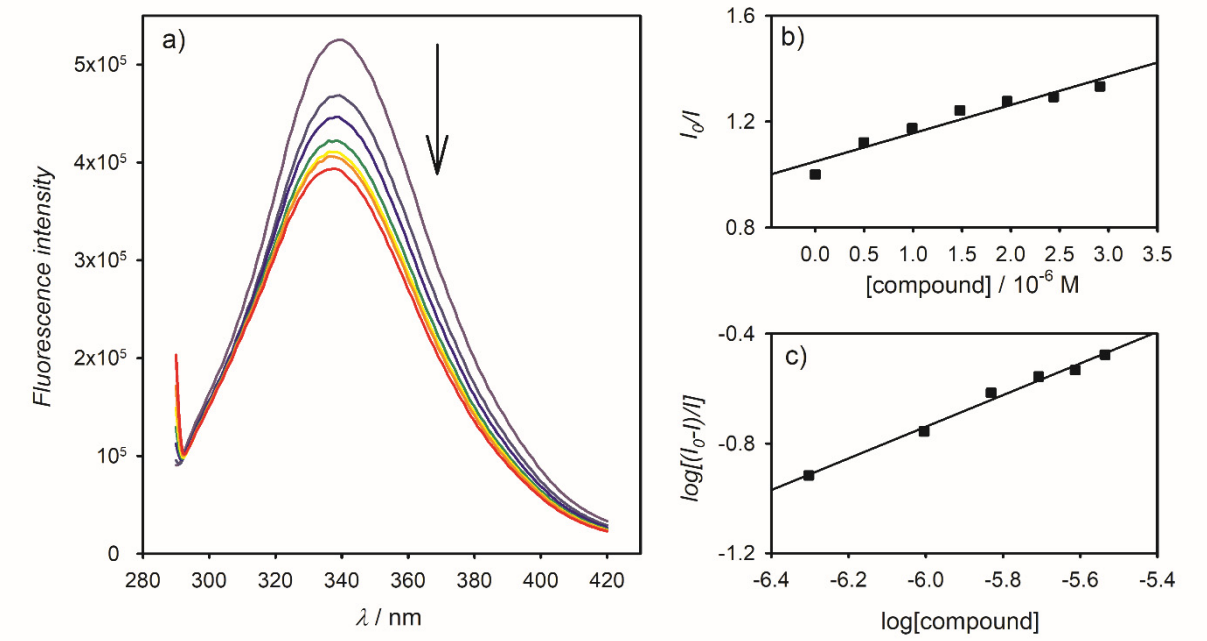


Figure S11. Interaction of $[\{RuCl_2(p\text{-cymene})\}_2(\mu\text{-dppb})]$ with BSA in 50 mM phosphate buffer pH 7.42: a) fluorescence quenching of BSA (2.93×10^{-5} M) in the presence of increasing concentration of complex; b) graphical determination of Stern–Volmer constant; c) graphical determination of binding constant and the number of binding sites.

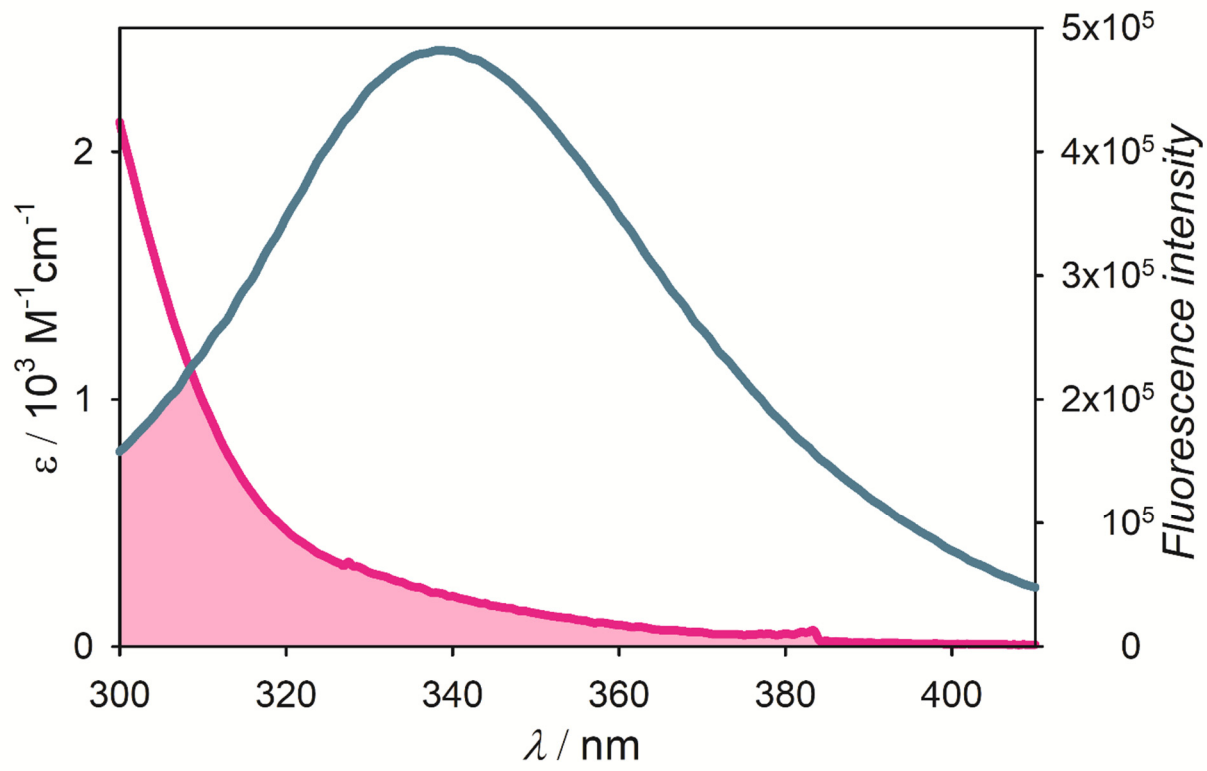


Figure S12. Overlap of the BSA emission spectrum and absorption spectrum of $[Au_2Cl_2(dppb)_2]$.

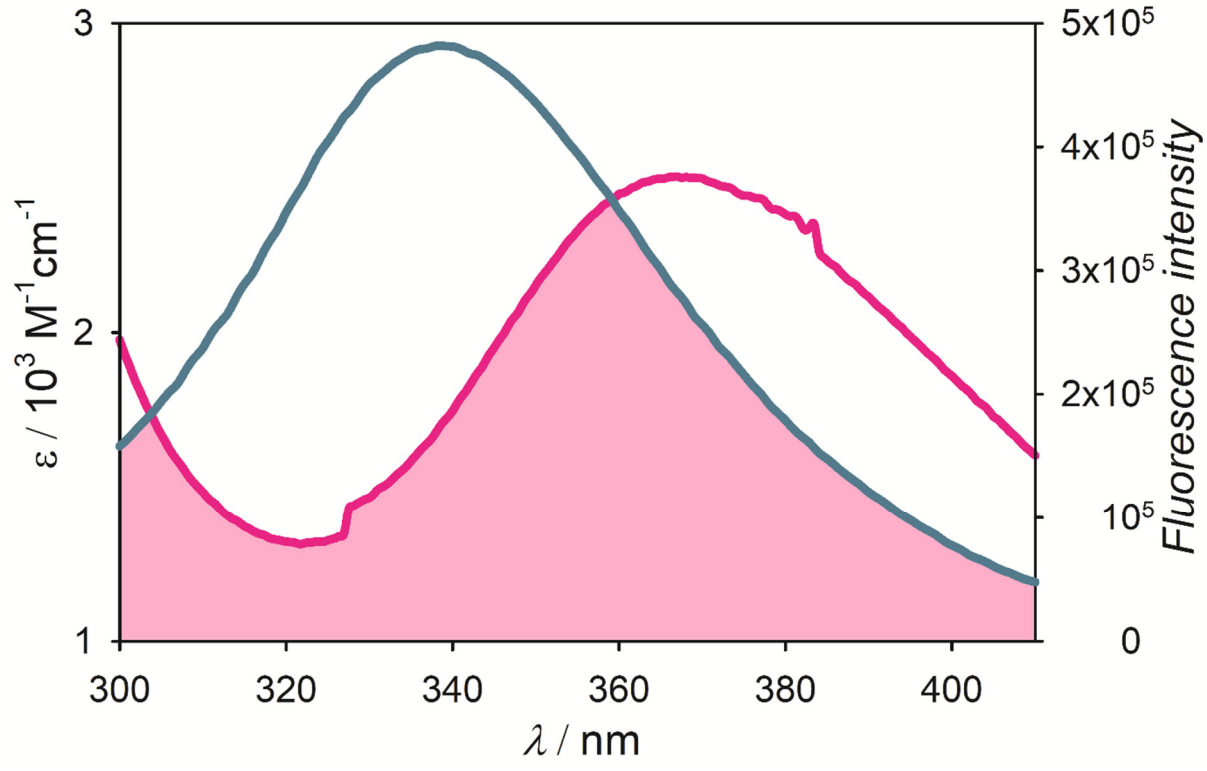


Figure S13. Overlap of the BSA emission spectrum and absorption spectrum of $[\{RuCl_2(p\text{-cymene})\}_2(\mu\text{-dppb})]$.